

ANNEALED DENOISING SCORE MATCHING: LEARNING ENERGY-BASED MODELS IN HIGH-DIMENSIONAL SPACES

Zengyi Li

Redwood Center for theoretical Neuroscience
 Department of Physics
 University of California Berkeley
 Berkeley, CA 94720, USA
 zengyi_li@berkeley.edu

Yubei Chen

Redwood Center for Theoretical Neuroscience
 Berkeley AI Research
 University of California Berkeley
 Berkeley, CA 94720, USA
 yubeic@berkeley.edu

Friedrich T. Sommer

Redwood Center for Theoretical Neuroscience
 Helen Wills Neuroscience Institute
 University of California Berkeley
 Berkeley, CA 94720, USA
 fsommer@berkeley.edu

ABSTRACT

Energy-Based Models (EBMs) outputs unmormalized log-probability values given data samples. Such an estimation is essential in a variety of applications such as sample generation, denoising, sample restoration, outlier detection, Bayesian reasoning, and many more. However, standard maximum likelihood training is computationally expensive due to the requirement of sampling the model distribution. Score matching potentially alleviates this problem, and denoising score matching (Vincent, 2011) is a particularly convenient version. However, previous works do not produce models capable of high quality sample synthesis in high dimensional datasets from random initialization. We believe that is because the score is only matched over a single noise scale, which corresponds to a small set in high-dimensional space. To overcome this limitation, here we instead learn an energy function using denoising score matching over all noise scales. When sampled from random initialization using Annealed Langevin Dynamics and single step denoising jump, our model produced high-quality samples comparable to state-of-the-art techniques such as GANs. The learned model also provide density information and set a new sample quality baseline in energy-based models. We further demonstrate that the proposed method generalizes well with an image inpainting task.

1 INTRODUCTION AND MOTIVATION

Treating data as stochastic samples from a probability distribution and developing models that can learn such distributions is at the core for solving a large variety of application problems, such as error correction/denoising (Vincent et al., 2010), outlier/novelty detection (Zhai et al., 2016; Choi and Jang, 2018), invariant pattern recognition, Bayesian reasoning (Welling and Teh, 2011) which relies on good data priors, and many others.

Energy-Based Models (EBMs) (LeCun et al., 2006; Ngiam et al., 2011) assign an energy $E(\mathbf{x})$ to each data point \mathbf{x} which implicitly defines a probability by the Boltzmann distribution $p_m(\mathbf{x}) = e^{-E(\mathbf{x})}/Z$. Sampling from this distribution can be used as a generative process that yield plausible samples of \mathbf{x} . Compared to other generative models, like GANs (Goodfellow et al., 2014), flow-based models (Dinh et al., 2015; Kingma and Dhariwal, 2018), or auto-regressive models (van den Oord et al., 2016; Ostrovski et al., 2018), energy-based models have significant advantages. First,

they provide explicit (unnormalized) density information, compositionality (Hinton, 1999; Haarnoja et al., 2017), better mode coverage (Kumar et al., 2019) and flexibility (Du and Mordatch, 2019). Second, they do not require special model architecture, unlike auto-regressive and flow-based models. Recently, Energy-based models has been successfully trained with maximum likelihood (Nijkamp et al., 2019; Du and Mordatch, 2019), but training can be very computationally demanding due to the need of sampling model distribution. Variants with a truncated sampling procedure have been proposed, such as contrastive divergence (Hinton, 2002). Such models learn much faster with the draw back of not exploring the state space thoroughly (Tieleman, 2008).

1.1 SCORE MATCHING, DENOISING SCORE MATCHING AND NEURAL EMPIRICAL BAYES

Score matching (Hyvärinen, 2005) circumvents the requirement of sampling the model distribution. In score matching, the score function is defined to be the gradient of log-density or the negative energy function. The expected L_2 norm of difference between the model score function and the data score function are minimized. One convenient way of using score matching is learning the energy function corresponding to a Gaussian kernel Parzen density estimator (Parzen, 1962) of the data: $p_{\sigma_0}(\tilde{\mathbf{x}}) = \int q_{\sigma_0}(\tilde{\mathbf{x}}|\mathbf{x})p(\mathbf{x})dx$. Though hard to evaluate, the data score is well defined: $s_d(\mathbf{x}) = \nabla_{\tilde{\mathbf{x}}} \log(p_{\sigma_0}(\tilde{\mathbf{x}}))$. And the corresponding objective is:

$$L_{SM}(\theta) = \mathbb{E}_{p_{\sigma_0}(\tilde{\mathbf{x}})} \|\nabla_{\tilde{\mathbf{x}}} \log(p_{\sigma_0}(\tilde{\mathbf{x}})) + \nabla_{\tilde{\mathbf{x}}} E(\tilde{\mathbf{x}}; \theta)\|^2 \quad (1)$$

Vincent (2011) studied the connection between denoising auto-encoder and score matching, and proved a remarkable result that the following objective, named *Denoising Score Matching*, is equivalent to the objective above:

$$L_{DSM}(\theta) = \mathbb{E}_{p_{\sigma_0}(\tilde{\mathbf{x}}, \mathbf{x})} \|\nabla_{\tilde{\mathbf{x}}} \log(q_{\sigma_0}(\tilde{\mathbf{x}}|\mathbf{x})) + \nabla_{\tilde{\mathbf{x}}} E(\tilde{\mathbf{x}}; \theta)\|^2 \quad (2)$$

Note that the Parzen density score is replaced by the derivative of log density of the single noise kernel $\nabla_{\tilde{\mathbf{x}}} \log(q_{\sigma}(\tilde{\mathbf{x}}|\mathbf{x}))$, which is much easier to evaluate. In the particular case of Gaussian noise $\log(q_{\sigma_0}(\tilde{\mathbf{x}}|\mathbf{x})) = -\frac{(\tilde{\mathbf{x}} - \mathbf{x})^2}{2\sigma_0^2} + C$ and:

$$L_{DSM}(\theta) = \mathbb{E}_{p_{\sigma_0}(\tilde{\mathbf{x}}, \mathbf{x})} \|\mathbf{x}_i - \tilde{\mathbf{x}}_i + \sigma_0^2 \nabla_{\tilde{\mathbf{x}}} E(\tilde{\mathbf{x}}_i; \theta)\|^2 \quad (3)$$

This objective (3) forces the energy gradient to align with the vector pointing from the noisy sample to the clean data sample, therefore it is named *Denoising score matching*. To optimize such an objective involving derivative of a function defined by a neural network, double backpropagation (Drucker and Le Cun, 1991) is needed, e.g. in (Kingma and LeCun, 2010). In Saremi et al. (2018), the authors first used the same technique to learn an energy function (density) defined by a deep neural network with denoising score matching. While learning the Parzen kernel density estimator under small noise was only proposed to analyze denoising autoencoder, Saremi et al. (2018) learned an energy-based model to match a Parzen estimator with a particular noise magnitude. Later, Song and Ermon (2019) learned a series of score estimators, each matching the score of a Parzen estimator with a different noise magnitude.

In this work, we combine some of the key ideas from Saremi et al. (2018); Saremi and Hyvärinen (2019); Song and Ermon (2019) and aim to learn an energy-based model using denoising score matching with multiple noise magnitudes. In Section 2, we first provide a geometric view to illustrate the training process of denoising score matching in high dimensional space, analyze its potential issues, and to motivate our own approach. Then we formulate *Annealed Denoising Score Matching* (ADSM), which is followed by a series of empirical results.

2 A GEOMETRIC VIEW

In Saremi and Hyvarinen (2019), author arrived at Equation 2 using a different theory based on Empirical Bayes estimator in the case of Gaussian noise. In the same paper learning of noise corrupted distribution was analyzed in high-dimensional case using measure concentration results. Here we develop upon this picture to further understand denoising score matching learning process.

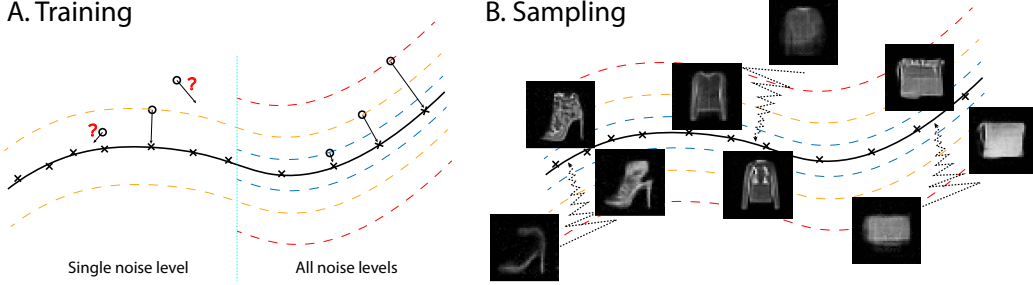


Figure 1: Illustration of anneal denoising score matching. A. During training, derivative of log-likelihood is forced to point toward data manifold, establishing energy difference between points within manifold and points outside. Note that energy is negative log-likelihood therefore energy is higher for point further away from data manifold. B. During annealed Langevin sampling, sample travel from outside data manifold to data manifold. Shown are singled step denoised sample during sampling of an energy function trained with ADSM on Fashion-MNIST (see text for details).

We adopt the common assumption that the data distribution to be learned is high-dimensional, but only has support around a relatively low-dimensional manifold (Tenenbaum et al., 2000; Roweis and Saul, 2000; Lawrence, 2005). This causes a problem that density, or the gradient of the density for data distribution is not defined outside the manifold, making it difficult to train a valid density model for the data distribution defined on the entire space. In Saremi and Hyvarinen (2019) and Song and Ermon (2019), authors analyzed this problem and motivated smoothing the data distribution with Gaussian kernel to alleviate this issue.

To understand the learning process in relation to the data manifold \mathcal{X} , we recall two elementary properties of random Gaussian vectors in high-dimensional spaces: First, the length distribution of random vectors becomes concentrated at $\sqrt{d}\sigma$ (Vershynin, 2018), where σ^2 is the variance of a single dimension. Second, a random vector is always close to orthogonal to a fixed vector (Tao, 2012). With these premises one can visualize the configuration of noisy and noiseless data points used in the learning of denoising score matching: A data point \mathbf{x} sampled from \mathcal{X} and its noisy version $\tilde{\mathbf{x}}$ always lie on a line which is almost perpendicular to the tangent space $T_{\mathbf{x}}\mathcal{X}$ and intersects \mathcal{X} at \mathbf{x} . Further, the distance vectors between $(\mathbf{x}, \tilde{\mathbf{x}})$ pairs all have similar length $\sqrt{d}\sigma$. As a consequence, the set of noisy data points concentrate on a set $\tilde{\mathcal{X}}_{\sqrt{d}\sigma, \epsilon}$ that has a distance with $(\sqrt{d}\sigma - \epsilon, \sqrt{d}\sigma + \epsilon)$ from the data manifold \mathcal{X} , where $\epsilon \ll \sqrt{d}\sigma$.

All told, performing denoising score matching learning with $(\mathbf{x}, \tilde{\mathbf{x}})$ pairs generated with a fixed noise level σ , which is the approach taken previously except in Song and Ermon (2019), will match the score on the set $\tilde{\mathcal{X}}_{\sqrt{d}\sigma, \epsilon}$ and enable de-noising of noisy points in $\tilde{\mathcal{X}}_{\sqrt{d}\sigma, \epsilon}$. However, the learning provides little information about the density outside this set, farther or closer to the data manifold, as noisy samples outside $\tilde{\mathcal{X}}_{\sqrt{d}\sigma, \epsilon}$ rarely appear in the training process. Similar issue also motivated Song and Ermon (2019) to use multiple noise scales. An illustration is presented in Figure 1A. Though $p_{\sigma_0}(\tilde{\mathbf{x}} \notin \tilde{\mathcal{X}}_{\sqrt{d}\sigma, \epsilon})$ is very small in high-dimensional space, the score in $\tilde{\mathcal{X}}_{\sqrt{d}\sigma, \epsilon}^C$ still plays a critical role in sampling from random noise. This may explain the difficulty previous models based on denoising score matching with single noise scale encountered when sampled with noise initialization. We demonstrate this experiment in Appendix C with multiple single noise magnitudes. This phenomenon in high-dimensional space is not sufficiently appreciated by the classical score matching objective, where the expectation almost confines score estimation to $\tilde{\mathcal{X}}_{\sqrt{d}\sigma, \epsilon}$. In fact, one way of motivating our proposed objective involves increasing this expectation to a larger set, see Appendix B for a more detailed discussion.

Another property of denoising score matching was observed in the denoising auto-encoder literature (Vincent et al., 2010; Karklin and Simoncelli, 2011) that with higher noise level the learned representation tend to have larger spatial scale. An plausible explanation is that a lot of natural signals have multi-scale structure with $1/f$ power characteristic, meaning that features at low spatial frequencies have larger signal power than features at high spacial frequencies (Field, 1987). Thus, a higher noise levels will wash away features above certain spacial frequencies, but insufficiently

corrupting features below certain spacial frequencies to drive learning. Thus, a model trained with only one noise level will only learn structures roughly of a single scale.

To illustrate this point, in Figure 1B we show some example of intermediate samples during annealed sampling process. Displayed are samples obtained by single step denoising from the noisy sample carrying different levels of noise. One can see that as the sample point approach the data manifold, more and more details are present in the denoised sample. We provide more result from this and similar experiment in Figure 3 and Figure F.1.

The analysis above suggest that its not sufficient to learn energy-based model with denoising score matching using a single noise scale, at least if high-quality sample synthesis is part of the goal for the learning. To achieve this while maintaining the speed advantage of score matching, we propose *annealed denoising score matching* (ADSM), a denoising score matching procedure using multiple noise levels. We expect this sampling-free learning method to shape an energy function that can drive samples anywhere in the state space towards high probability regions of the data. For sampling from the learned model, we propose *annealed Langevin dynamics* and additionally use single step denoise jump. We show that our model generates high-quality samples similar in quality to the-state-of-the-art image generation techniques, such as GANs (Goodfellow et al., 2014), as well as providing density information.

3 ENERGY-BASED MODEL WITH ANNEALED DENOISING SCORE MATCHING

3.1 ANNEALED DENOISING SCORE MATCHING

Motivated by the geometric view, we strive to learn an energy function that captures the structure of data over different scales by introducing different levels of Gaussian noise corruptions.

The data distribution over different noise scales can be expressed as $p_{\sigma_0, T}(\tilde{\mathbf{x}}) = \int q_{\sigma_0, T}(\tilde{\mathbf{x}}|\mathbf{x})p(\mathbf{x})dx$, where $q_{\sigma_0, T}(\tilde{\mathbf{x}}|\mathbf{x}) = \mathcal{N}(\tilde{\mathbf{x}}|\mathbf{x}; T\sigma_0^2 I_d)$ and T is the temperature parameter that scales the size of Gaussian kernel (Mehrjou et al., 2017). Running traditional denoising score matching for different noise temperatures would lead to different energy functions $E_T(\tilde{\mathbf{x}}; \theta)$ for each noise scale. This is undesirable, as the number of free model parameters will be multiplied by the number of different temperatures used during learning, and it is unclear how to obtain density information from such a set of different energy functions. In Song and Ermon (2019), the authors cleverly used noise-conditioned layer to superimpose score functions under different noise levels together in one network. This avoids the parameter multiplication problem but still don't produce a density model. As an alternative, we propose a model in which the energy functions for different temperatures are collapsed into a single function $E(\tilde{\mathbf{x}}; \theta)$. We borrow intuition from physics and simply set $E_T(\tilde{\mathbf{x}}; \theta) = E(\tilde{\mathbf{x}}; \theta)/T$ and use denoising score matching (2) to approximate $\log(p_{\sigma_0, T}(\tilde{\mathbf{x}}))$ by $E(\tilde{\mathbf{x}}; \theta)/T$:

$$L_{DSM}(\theta; T) = \mathbb{E}_{p_{\sigma_0, T}(\tilde{\mathbf{x}}, \mathbf{x})} \|\nabla_{\tilde{\mathbf{x}}} \log(q_{\sigma_0, T}(\tilde{\mathbf{x}}|\mathbf{x})) + \nabla_{\tilde{\mathbf{x}}} E(\tilde{\mathbf{x}}; \theta)/T\|^2 \quad (4)$$

In the case of Gaussian noise (3) and by combining objective (4) over a temperature range gives the objective of *Annealed Denoising Score Matching*:

$$L_{ADSM}(\theta) = \sum_T l(T) \mathbb{E}_{p_{\sigma_0, T}(\tilde{\mathbf{x}}, \mathbf{x})} \|\mathbf{x}_i - \tilde{\mathbf{x}}_{i, T} + \sigma_0^2 \nabla_{\tilde{\mathbf{x}}} E(\tilde{\mathbf{x}}_{i, T}; \theta)\|^2 \quad (5)$$

where $l(T)$ is a weighting function that normalizes terms from different temperatures. Here \mathbf{x}_i and $\tilde{\mathbf{x}}_{i, T}$ denote a clean data point and its corrupted version with a noise level corresponding to temperature T , i.e. $q_{\sigma_0, T}(\tilde{\mathbf{x}}|\mathbf{x}) = \mathcal{N}(\tilde{\mathbf{x}}|\mathbf{x}; T\sigma_0^2 I_d)$. Since the difference $\mathbf{x}_i - \tilde{\mathbf{x}}_{i, T}$ scales linearly with the noise level, after successful training, we expect $\nabla_{\tilde{\mathbf{x}}} E(\tilde{\mathbf{x}}_{i, T}; \theta)$ to scale similarly, thus the energy $E(\tilde{\mathbf{x}}_{i, T}; \theta)$ should be roughly quadratic along the noise direction. We present a plausible physics illustration of the learned energy function in Appendix A. Equation 5 also admits a different interpretation where the score of $p_{\sigma_0}(\tilde{\mathbf{x}})$ is still matched with $\nabla_{\tilde{\mathbf{x}}} E(\tilde{\mathbf{x}}; \theta)$ but the expectation w.r.t. $p_{\sigma_0}(\tilde{\mathbf{x}})$ in Equation 1 is replace by Gaussian scale mixture noise rather than a single-magnitude noise, see Appendix B for a more detailed discussion.

The ADSM objective could be seen as a means to obtain an estimation of the true data distribution $p(\mathbf{x})$ via the Boltzmann distribution defined by the energy function $E(\mathbf{x}; \theta)/T$, in the limit of $T \rightarrow 0$.

It has to be emphasized that modeling $\log(p_{\sigma_0, T}(\tilde{\mathbf{x}}))$ by $E(\tilde{\mathbf{x}}; \theta)/T$ is not be achieved approximately. Specifically, one can think of $p_{\sigma_0, T}(\tilde{\mathbf{x}})$ as a mixture of Gaussians, as $\log(p_{\sigma_0, T}(\tilde{\mathbf{x}}))/T$ is not the same function for different T . Therefore it is hard to write down the exact functional form of $E(\tilde{\mathbf{x}}; \theta)$ with the objective Equation 5. In Appendix B, we show in Equation (*) where the approximation is made. Despite the theoretical difficulty, we argue the proposed learning method is desirable by noting the following: 1) Learning is tractable and fast because, like the original denoising score matching, training does not require sampling from the model. 2) As the gradient of energy function is required to point away from the noisy data point in the opposite direction of the clean samples, the noisy sample will have higher energy, and thus lower probability than the clean data point. 3) When temperature increases, the equilibrium distribution will have fewer and fewer modes, as expected from physical intuition. This statement is true since $E(\mathbf{x}; \theta)/T$ is trained to match $\log(p_{\sigma_0, T}(\tilde{\mathbf{x}}))$ and the latter was shown to possess a monotonically decreasing number of modes as T increases (Lindeberg, 2011). 4) Because training is performed over a range of temperatures, the resulting energy function will naturally permit annealing sampling which helps with mode exploration.

It seems that the temperature range and σ_0 in (5) are both important hyper-parameters. However, all that matters is the range of $T\sigma_0^2$, the range of noise magnitude we apply. Ideally we want our model to work across all noise levels, but applying denoising score matching to very large or very small noise is rather pointless. For very large noise the original sample's information is completely lost. Conversely, in the limit of small noise, the noisy sample is virtually indistinguishable from real data. In neither case can one expect to learn an informative gradient. Thus, in practice the noise range needs only be chosen broad enough to encourage learning of data features over all scales.

3.2 SAMPLING BY ANNEALED LANGEVIN DYNAMICS AND JUMP

In Saremi and Hyvarinen (2019), the energy function corresponding to Parzen density estimator of a single noise scale is sampled by Langevin dynamics, and clean sample can be obtained using single step denoise jump. We extend this approach to sample from our learned energy function with annealed Langevin dynamics, as our energy function is trained over all temperatures (noise levels). Additionally we use the same single step denoise jump.

Simulated annealing (Kirkpatrick et al., 1983; Neal, 2001) has been successfully applied to challenging computational problems, such as combinatorial optimization. In essence, the mode exploration in an objective function can be improved by sampling first at high temperature and then cooling down gradually. Langevin dynamics (Welling and Teh, 2011) has been applied to sampling from neural network energy functions (Du and Mordatch, 2019; Nijkamp et al., 2019). However, they reported difficulty with mode exploration or the need for very large number of sampling steps. To improve mode exploration even with small numbers of sampling steps, we propose Annealed Langevin dynamics. In this sampling process the temperature parameter in the Langevin dynamics is adjusted from high to low according to an annealing schedule.

In the model of a physical particle undergoing Brownian motion, temperature in its Langevin equation enters as a \sqrt{T} factor in front of the noise term. Adopting this yields the following sampling process:

$$\mathbf{x}_{t+1} = \mathbf{x}_t - \frac{\epsilon^2}{2} \nabla_{\mathbf{x}} E(\mathbf{x}_t; \theta) + \epsilon \sqrt{T_t} \mathcal{N}(0, I_d) \quad (6)$$

where T_t follows some annealing schedule, and ϵ denotes step length, which is fixed. During sampling, samples behave very much like physical particles under Brownian motion in a potential field. Because the particles have average energies close to their current thermic energy, they explore the state space at different distances from data manifold depending on temperature. Eventually, they settle somewhere on the data manifold. The behavior of the particle's energy value during a typical annealing process is depicted in Appendix Figure G.1B. If the obtained sample is still noisy, we can make a single step gradient denoise jump to improve sample quality:

$$\mathbf{x}_{clean} = \mathbf{x}_{noisy} - \sigma_0^2 \nabla_{\mathbf{x}} E(\mathbf{x}_{noisy}; \theta) \quad (7)$$

This denoising procedure can be applied to noisy sample with any level of Gaussian noise because in our model the gradient automatically has the right magnitude to denoise the sample. This process is also justified by the Empirical Bayes interpretation of this denoising process, as noted in Saremi and Hyvarinen (2019).



Figure 2: Samples from our model trained on Fashion MNIST, CelebA and CIFAR-10. See Figure F.3 and Figure F.4 in Appendix for more samples and comparison with training data.

In the NCSN model (Song and Ermon, 2019), author also proposed annealed Langevin dynamics, which is best interpreted as sequentially sampling a series of distributions. Our formulation differs as our algorithm samples one energy function at different temperatures.

4 IMAGE MODELING RESULTS

Training and Sampling Details. The proposed energy-based model is trained on standard image datasets, namely MNIST, Fashion MNIST, CelebA (Liu et al., 2015) and CIFAR-10 (Krizhevsky et al., 2009). During training we set $\sigma_0 = 0.1$ and train over a noise range of $\sqrt{T}\sigma_0 \in [0.05, 1.2]$, with the noise uniformly spaced on the batch dimension, for MNIST and Fashion MNIST we used geometrically distributed noise in the range $[0.1, 3]$. $l(T)$ is set to $1/T$ at all times to make each terms in the objective from different noise scale roughly the same size. We fix the batch size to 128 and use the Adam optimizer with a learning rate of 5×10^{-5} . For MNIST and Fashion MNIST, we use a 12-Layer ResNet with 64 filters, for the CelebA and CIFAR-10 data sets we used a 18-Layer ResNet with 128 filters (He et al., 2016; Zagoruyko and Komodakis, 2016). No normalization layer was used in any of the networks. We designed the output layer of all networks to take a generalized quadratic form (Fan et al., 2018), because the energy function is anticipated to be approximately quadratic with respect to the noise level, we found this modification to boost the performance significantly. For more detail on training and model architecture, see Appendix E. One notable result is that since our training method does not involve sampling, we achieved a speed up of roughly an order of magnitude compared to the common maximum-likelihood training¹. Our method thus enables the training of energy-based models even when limited computational resources prohibit maximum likelihood methods.

We found that the choice of the maximum noise level has little effect on learning as long as it is large enough to encourage learning of the longest range features in the data. However, as expected, learning with too small or too large noise levels is not beneficial and can even destabilize the training process. Further, our method appeared to be relatively insensitive to how the noise levels are distributed over a chosen range. Geometrically spaced noise as in (Song and Ermon, 2019) and linearly spaced noise both work, although in our case learning with linearly spaced noise was somewhat more robust.

For sampling the learned energy function we used annealed Langevin dynamics with an empirically optimized annealing schedule, see Figure G.1 B for the particular shape of annealing schedule we used. In contrast, annealing schedules with theoretical guaranteed convergence property takes extremely long (Geman and Geman, 1984). For step length ϵ we generally used 0.02, although any value within the range $[0.015, 0.05]$ seemed to work fine. After annealing process we perform a single step denoising jump to further enhance sample quality.

¹For example, on a single GPU, training MNIST with 12-layer Resnet takes 0.3s per batch with our method, while maximum likelihood training with a modest 30 Langevin step per weight update takes 3s per batch.

²Author reported difficulties evaluating Likelihood

³Upper Bound obtained by Reverse AIS

Table 1: Unconditional Inception score, FID scores and Likelihoods for CIFAR-10

Model	IS	FID	Likelihood	NNL (bits/dim)
iResNet (Behrmann et al., 2019)	-	65.01	Yes	3.45
PixelCNN (van den Oord et al., 2016)	4.60	65.93	Yes	3.14
PixelIQN (Ostrovski et al., 2018)	5.29	49.46	Yes	-
Residual Flow (Chen et al., 2019)	-	46.37	Yes	3.28
GLOW (Kingma and Dhariwal, 2018)	-	46.90	Yes	3.35
EBM (ensemble) (Du and Mordatch, 2019)	6.78	38.2	Yes(density)	- ²
SNGAN (Miyato et al., 2018)	8.22	21.7	No	-
ADSM(Ours)	8.31	31.7	Yes(density)	-0.96 ³
NCSN (Song and Ermon, 2019)	8.91	25.32	No	-

Unconditional Image Generation. We demonstrate the generative ability of our model by displaying samples obtained by annealed Langevin sampling and single step denoise jump. We evaluated 50k sampled images after training on CIFAR-10 with two performance scores, Inception (Salimans et al., 2016) and FID (Heusel et al., 2017). We achieved Inception Score of 8.31 and FID of 31.7, comparable to modern GAN approaches. Scores for CelebA dataset are not reported here as they are not commonly reported and may depend on the specific pre-processing used. More samples and training images are provided in Appendix for visual inspection. We believe that visual assessment is still essential because of issues with the Inception score (Barratt and Sharma, 2018). Indeed, we also found that the visually impressive samples was not the one achieving the highest Inception Score.

Although overfitting is not a common concern for generative models, we still tested our model for overfitting. We found no indication for overfitting by comparing model samples with their nearest neighbors in the data set, see Figure D.1 in Appendix.

Mode Coverage. We repeated with our model the 3 channel MNIST mode coverage experiment similar to the one in Kumar et al. (2019). An energy-based model was trained on 3-channel data where each channel is a random MNIST digit. Then 8000 samples were taken from the model and each channel is classified using a small MNIST classifier network. We obtained results of the 966 modes, comparable to GAN approaches. Training was successful and our model assigned low energy to all the learned modes, but some modes were not accessed during sampling, likely due to the Langevin Dynamics failing to explore these modes. A better sampling technique such as Neal et al. (2011) or a Maximum Entropy Generator (Kumar et al., 2019) could improve this result.

Image Inpainting. Image inpainting can be achieved with our model by clamping part of the image to ground truth and performing the same annealed Langevin and Jump sampling procedure on the missing part of the image. Noise appropriate to the sampling temperature need to be added to the clamped inputs. The quality of inpainting results of our model trained on CelebA and CIFAR-10 can be assessed in Figure 3. For CIFAR inpainting we used test set,

Log likelihood estimation. For energy-based models the log density can be obtained after estimating the partition function with Annealed Importance Sampling (AIS) (Salakhutdinov and Murray, 2008) or Reverse AIS (Burda et al., 2015). In our experiment on CIFAR-10 model, similar to report in Du and Mordatch (2019), there’s still a substantial gap between AIS and Reverse AIS estimation after very substantial computational effort. In Table 1, We report result from Reverse AIS as it tends to over-estimate the partition function thus underestimate the density. Note that although density values and likelihood values are not directly comparable, we list them together due to the sheer lack of density model on CIFAR-10.

We also report density of 1.21 bits/dim on MNIST dataset, and we refer readers to Du and Mordatch (2019) for comparison to other models on this dataset. More details on this experiment is provided in the Appendix.

Outlier Detection. Choi and Jang (2018) and Nalisnick et al. (2019) have reported intriguing behavior of high dimensional density models on out of distribution samples. Specifically, they showed

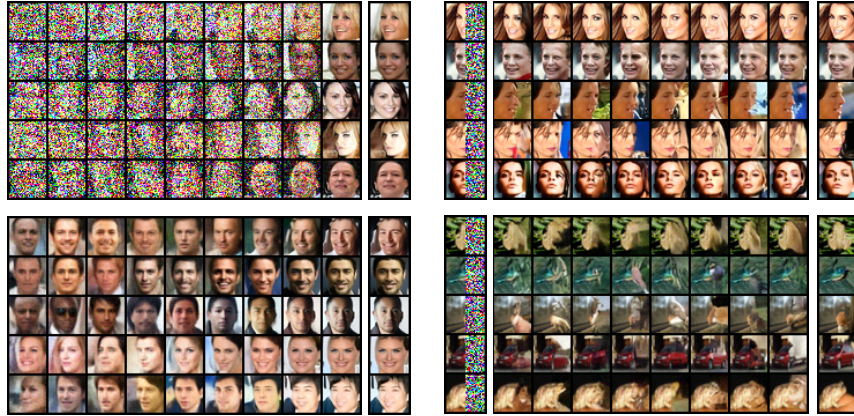


Figure 3: Demonstration of the sampling process (left), and image inpainting (right). The sampling process is shown with Gaussian noise (top left), and denoised by single step gradient jump (lower left). The column next to sampling process shows samples after the last denoising jump at the end of sampling. Inpainting results are shown next to initial image (left column) and the ground truth image (right column).

that a lot of models assign higher likelihood to out of distribution samples than real data samples. We investigated whether our model behaves similarly.

Our energy function is only trained outside the data manifold where samples are noisy, so the energy value at clean data points may not always be well behaved. Therefore, we added noise with magnitude σ_0 before measuring the energy value. We report that our network behaves similarly to previous likelihood models that it assigns lower energy, thus higher density, to some OOD samples. We show one example of this phenomenon in Appendix Figure G.1A.

We also attempted to use the denoise performance, or the objective function to perform outlier detection. Intriguingly, it also behaves similarly as using energy value, as denoise performance seems to correlate more with the variance of original image rather than the content of the image.

5 DISCUSSION

Our approach is conceptually similar to the idea of combining denoising autoencoder and annealing (Geras and Sutton, 2015; Chandra and Sharma, 2014; Zhang and Zhang, 2018) though they were proposed in the context of pre-training neural networks for classification applications. Previous efforts of learning energy-based models with score matching (Kingma and LeCun, 2010; Song et al., 2019) were either computationally intensive or unable to produce high-quality samples comparable to those obtained by other generative models such as GANs. Saremi et al. (2018) and Saremi and Hyvarinen (2019) trained energy-based model with denoising score matching objective but the resulting models cannot perform sample synthesis from random noise initializations.

We provide analysis and empirical results both suggesting that the limitation of previous denoising score matching models is due to the objective doesn't sufficiently appreciate low-density regions. To remedy this issue we proposed a learning procedure using a wide range of different noise scales, which we named *Annealed Denoising Score Matching*. Despite being an approximation, the models learned with ADSM is capable of denoising, producing high-quality samples from random noise, and performing image inpainting. They achieve those while providing density information, being an order of magnitude faster over maximum likelihood method during training, and admitting a more efficient annealed Langevin sampling procedure.

Our approach is perhaps most closely related to the NCSN model (Song and Ermon, 2019), a network that is also trained by denoising score matching with noisy samples corrupted with Gaussian noise at different scales. In our notation, this model essentially learns $p_{\sigma_0, T}(\tilde{\mathbf{x}})$ for each T as a separate model. In addition to the input image, it receives a signal that represents the noise scale explicitly, thus output score corresponding to the specified noise scale. Our model differs in that it

learns one energy model for all noise scales (temperatures), thus it can perform single-step denoising independent of the noise scale. Moreover, our models provide density information, whereas it is not obvious how to transform the representation from the NCSN models into a density. The annealed Langevin dynamic sampling proposed in this paper also differs from the one proposed along with the NCSN model, reflecting the difference in model design. Thus, our model provides an unique combination of density information with high-quality sample generation.

ACKNOWLEDGEMENTS

We thank Saeed Saremi and Bruno Olshausen for many helpful comments and suggestions. This work was funded by NSF award 1718991, and by an INRC research grant from Intel Corporation.

REFERENCES

Shane Barratt and Rishi Sharma. A note on the inception score. *arXiv preprint arXiv:1801.01973*, 2018.

Jens Behrmann, Will Grathwohl, Ricky T. Q. Chen, David Duvenaud, and Jörn-Henrik Jacobsen. Invertible residual networks. In *Proceedings of the 36th International Conference on Machine Learning, ICML 2019, 9-15 June 2019, Long Beach, California, USA*, pages 573–582, 2019.

Yuri Burda, Roger Grosse, and Ruslan Salakhutdinov. Accurate and conservative estimates of mrf log-likelihood using reverse annealing. In *Artificial Intelligence and Statistics*, pages 102–110, 2015.

B Chandra and Rajesh Kumar Sharma. Adaptive noise schedule for denoising autoencoder. In *International conference on neural information processing*, pages 535–542. Springer, 2014.

Ricky TQ Chen, Jens Behrmann, David Duvenaud, and Jörn-Henrik Jacobsen. Residual flows for invertible generative modeling. *arXiv preprint arXiv:1906.02735*, 2019.

Hyunsun Choi and Eric Jang. Generative ensembles for robust anomaly detection. *arXiv preprint arXiv:1810.01392*, 2018.

Laurent Dinh, David Krueger, and Yoshua Bengio. NICE: non-linear independent components estimation. In *3rd International Conference on Learning Representations, ICLR 2015, San Diego, CA, USA, May 7-9, 2015, Workshop Track Proceedings*, 2015.

Harris Drucker and Yann Le Cun. Double backpropagation increasing generalization performance. In *IJCNN-91-Seattle International Joint Conference on Neural Networks*, volume 2, pages 145–150. IEEE, 1991.

Yilun Du and Igor Mordatch. Implicit generation and generalization in energy-based models. *arXiv preprint arXiv:1903.08689*, 2019.

Fenglei Fan, Wenxiang Cong, and Ge Wang. A new type of neurons for machine learning. *International journal for numerical methods in biomedical engineering*, 34(2):e2920, 2018.

David J. Field. Relations between the statistics of natural images and the response properties of cortical cells. *J. Opt. Soc. Am. A*, 4(12):2379–2394, Dec 1987.

Stuart Geman and Donald Geman. Stochastic relaxation, gibbs distributions, and the bayesian restoration of images. *IEEE Transactions on pattern analysis and machine intelligence*, (6): 721–741, 1984.

Krzysztof J. Geras and Charles A. Sutton. Scheduled denoising autoencoders. In *3rd International Conference on Learning Representations, ICLR 2015, San Diego, CA, USA, May 7-9, 2015, Conference Track Proceedings*, 2015.

Ian Goodfellow, Jean Pouget-Abadie, Mehdi Mirza, Bing Xu, David Warde-Farley, Sherjil Ozair, Aaron Courville, and Yoshua Bengio. Generative adversarial nets. In *Advances in neural information processing systems*, pages 2672–2680, 2014.

Tuomas Haarnoja, Haoran Tang, Pieter Abbeel, and Sergey Levine. Reinforcement learning with deep energy-based policies. In *Proceedings of the 34th International Conference on Machine Learning-Volume 70*, pages 1352–1361. JMLR. org, 2017.

Kaiming He, Xiangyu Zhang, Shaoqing Ren, and Jian Sun. Deep residual learning for image recognition. In *Proceedings of the IEEE conference on computer vision and pattern recognition*, pages 770–778, 2016.

Martin Heusel, Hubert Ramsauer, Thomas Unterthiner, Bernhard Nessler, and Sepp Hochreiter. Gans trained by a two time-scale update rule converge to a local nash equilibrium. In *Advances in Neural Information Processing Systems*, pages 6626–6637, 2017.

Geoffrey E Hinton. Products of experts. 1999.

Geoffrey E Hinton. Training products of experts by minimizing contrastive divergence. *Neural computation*, 14(8):1771–1800, 2002.

Aapo Hyvärinen. Estimation of non-normalized statistical models by score matching. *Journal of Machine Learning Research*, 6(Apr):695–709, 2005.

Yan Karklin and Eero P Simoncelli. Efficient coding of natural images with a population of noisy linear-nonlinear neurons. In *Advances in neural information processing systems*, pages 999–1007, 2011.

Diederik P. Kingma and Yann LeCun. Regularized estimation of image statistics by score matching. In *Advances in Neural Information Processing Systems 23: 24th Annual Conference on Neural Information Processing Systems 2010. Proceedings of a meeting held 6-9 December 2010, Vancouver, British Columbia, Canada.*, pages 1126–1134, 2010.

Durk P Kingma and Prafulla Dhariwal. Glow: Generative flow with invertible 1x1 convolutions. In *Advances in Neural Information Processing Systems*, pages 10215–10224, 2018.

Scott Kirkpatrick, C Daniel Gelatt, and Mario P Vecchi. Optimization by simulated annealing. *science*, 220(4598):671–680, 1983.

Alex Krizhevsky, Geoffrey Hinton, et al. Learning multiple layers of features from tiny images. Technical report, Citeseer, 2009.

Rithesh Kumar, Anirudh Goyal, Aaron Courville, and Yoshua Bengio. Maximum entropy generators for energy-based models. *arXiv preprint arXiv:1901.08508*, 2019.

Neil Lawrence. Probabilistic non-linear principal component analysis with gaussian process latent variable models. *Journal of machine learning research*, 6(Nov):1783–1816, 2005.

Yann LeCun, Sumit Chopra, Raia Hadsell, M Ranzato, and F Huang. A tutorial on energy-based learning. *Predicting structured data*, 1(0), 2006.

Tony Lindeberg. Generalized gaussian scale-space axiomatics comprising linear scale-space, affine scale-space and spatio-temporal scale-space. *Journal of Mathematical Imaging and Vision*, 40(1): 36–81, 2011.

Ziwei Liu, Ping Luo, Xiaogang Wang, and Xiaoou Tang. Deep learning face attributes in the wild. In *Proceedings of the IEEE international conference on computer vision*, pages 3730–3738, 2015.

Arash Mehrjou, Bernhard Schölkopf, and Saeed Saremi. Annealed generative adversarial networks. *arXiv preprint arXiv:1705.07505*, 2017.

Takeru Miyato, Toshiki Kataoka, Masanori Koyama, and Yuichi Yoshida. Spectral normalization for generative adversarial networks. In *6th International Conference on Learning Representations, ICLR 2018, Vancouver, BC, Canada, April 30 - May 3, 2018, Conference Track Proceedings*, 2018.

Eric T. Nalisnick, Akihiro Matsukawa, Yee Whye Teh, Dilan Görür, and Balaji Lakshminarayanan. Do deep generative models know what they don't know? In *7th International Conference on Learning Representations, ICLR 2019, New Orleans, LA, USA, May 6-9, 2019*, 2019.

Radford M Neal. Annealed importance sampling. *Statistics and computing*, 11(2):125–139, 2001.

Radford M Neal et al. Mcmc using hamiltonian dynamics. *Handbook of markov chain monte carlo*, 2(11):2, 2011.

Jiquan Ngiam, Zhenghao Chen, Pang W Koh, and Andrew Y Ng. Learning deep energy models. In *Proceedings of the 28th international conference on machine learning (ICML-11)*, pages 1105–1112, 2011.

Erik Nijkamp, Mitch Hill, Tian Han, Song-Chun Zhu, and Ying Nian Wu. On the anatomy of mcmc-based maximum likelihood learning of energy-based models. *arXiv preprint arXiv:1903.12370*, 2019.

Georg Ostrovski, Will Dabney, and Rémi Munos. Autoregressive quantile networks for generative modeling. In *Proceedings of the 35th International Conference on Machine Learning, ICML 2018, Stockholm, Sweden, July 10-15, 2018*, pages 3933–3942, 2018.

Emanuel Parzen. On estimation of a probability density function and mode. *The Annals of Mathematical Statistics*, 33(3):1065–1076, 1962.

Sam T Roweis and Lawrence K Saul. Nonlinear dimensionality reduction by locally linear embedding. *science*, 290(5500):2323–2326, 2000.

Stuart J Russell and Peter Norvig. *Artificial intelligence: a modern approach*. Malaysia; Pearson Education Limited., 2016.

Ruslan Salakhutdinov and Iain Murray. On the quantitative analysis of deep belief networks. In *Proceedings of the 25th international conference on Machine learning*, pages 872–879. ACM, 2008.

Tim Salimans, Ian Goodfellow, Wojciech Zaremba, Vicki Cheung, Alec Radford, and Xi Chen. Improved techniques for training gans. In *Advances in neural information processing systems*, pages 2234–2242, 2016.

Saeed Saremi and Aapo Hyvarinen. Neural empirical bayes. *arXiv preprint arXiv:1903.02334*, 2019.

Saeed Saremi, Arash Mehrjou, Bernhard Schölkopf, and Aapo Hyvärinen. Deep energy estimator networks. *arXiv preprint arXiv:1805.08306*, 2018.

Yang Song and Stefano Ermon. Generative modeling by estimating gradients of the data distribution. *arXiv preprint arXiv:1907.05600*, 2019.

Yang Song, Sahaj Garg, Jiaxin Shi, and Stefano Ermon. Sliced score matching: A scalable approach to density and score estimation. In *Proceedings of the Thirty-Fifth Conference on Uncertainty in Artificial Intelligence, UAI 2019, Tel Aviv, Israel, July 22-25, 2019*, page 204, 2019.

Terence Tao. *Topics in random matrix theory*, volume 132. American Mathematical Soc., 2012.

Joshua B Tenenbaum, Vin De Silva, and John C Langford. A global geometric framework for nonlinear dimensionality reduction. *science*, 290(5500):2319–2323, 2000.

Tijmen Tieleman. Training restricted boltzmann machines using approximations to the likelihood gradient. In *Proceedings of the 25th international conference on Machine learning*, pages 1064–1071. ACM, 2008.

Aäron van den Oord, Nal Kalchbrenner, and Koray Kavukcuoglu. Pixel recurrent neural networks. In *Proceedings of the 33rd International Conference on Machine Learning, ICML 2016, New York City, NY, USA, June 19-24, 2016*, pages 1747–1756, 2016.

Roman Vershynin. *High-dimensional probability: An introduction with applications in data science*, volume 47. Cambridge University Press, 2018.

Pascal Vincent. A connection between score matching and denoising autoencoders. *Neural computation*, 23(7):1661–1674, 2011.

Pascal Vincent, Hugo Larochelle, Isabelle Lajoie, Yoshua Bengio, and Pierre-Antoine Manzagol. Stacked denoising autoencoders: Learning useful representations in a deep network with a local denoising criterion. *Journal of machine learning research*, 11(Dec):3371–3408, 2010.

Martin J Wainwright and Eero P Simoncelli. Scale mixtures of gaussians and the statistics of natural images. In *Advances in neural information processing systems*, pages 855–861, 2000.

Max Welling and Yee W Teh. Bayesian learning via stochastic gradient langevin dynamics. In *Proceedings of the 28th international conference on machine learning (ICML-11)*, pages 681–688, 2011.

Sergey Zagoruyko and Nikos Komodakis. Wide residual networks. *arXiv preprint arXiv:1605.07146*, 2016.

Shuangfei Zhai, Yu Cheng, Weining Lu, and Zhongfei Zhang. Deep structured energy based models for anomaly detection. In *Proceedings of the 33nd International Conference on Machine Learning, ICML 2016, New York City, NY, USA, June 19-24, 2016*, pages 1100–1109, 2016.

Qianjun Zhang and Lei Zhang. Convolutional adaptive denoising autoencoders for hierarchical feature extraction. *Frontiers of Computer Science*, 12(6):1140–1148, 2018.

A A PHYSICS ANALOGY TO UNDERSTAND THE ADSM OBJECTIVE FUNCTION

Here we provide a concrete physics picture of the energy function learned by annealed score matching. Given a data manifold X , we define the energy function as:

$$E^*(d) = \frac{1}{2}kd^2 \quad (8)$$

where $d = \|\tilde{\mathbf{x}} - \text{proj}_X(\tilde{\mathbf{x}})\|$ and $\text{proj}_X(\tilde{\mathbf{x}})$ is the projection operator to the data manifold X . One can easily verify that this is an energy function and describes a generalized Hookean spring system. At any point $\tilde{\mathbf{x}}$ away from the data manifold X , the force F is:

$$F = -\nabla_{\tilde{\mathbf{x}}} E^*(\tilde{\mathbf{x}}) = k(\tilde{\mathbf{x}} - \text{proj}_X(\tilde{\mathbf{x}})) \quad (9)$$

as Figure A.1 shows.

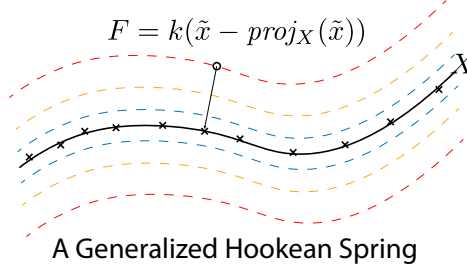


Figure A.1: Generalized Hookean spring system, where the force F at any noise-corrupted point $\tilde{\mathbf{x}}$ points towards its projection $\text{proj}_X(\tilde{\mathbf{x}})$ on the data manifold X and is proportional to the distance from $\tilde{\mathbf{x}}$ to X .

In high dimensional space, given a data point \mathbf{x} and a Gaussian noise corrupted version $\tilde{\mathbf{x}}$, $\tilde{\mathbf{x}} - \mathbf{x}$ provides a good approximation to $\tilde{\mathbf{x}} - \text{proj}_X(\tilde{\mathbf{x}})$. Thus, by matching the score to $\tilde{\mathbf{x}} - \mathbf{x}$ at every noisy point, the ADSM objective is an approximation to the energy defined by Equation 8, trained at different distances. Empirically, we also verified that the $E(\tilde{\mathbf{x}}; \theta)$ increases in quadratic fashion w.r.t. $\|\tilde{\mathbf{x}} - \mathbf{x}\|$.

B ADSM OBJECTIVE

In this section, we provide a formal discussion of the ADSM objective and suggest it as an improved score matching formulation in high-dimensional space.

Vincent (2011) illustrated the connection between the model score $-\nabla_{\tilde{\mathbf{x}}} E(\tilde{\mathbf{x}}; \theta)$ with the score of Parzen window density estimator $\nabla_{\tilde{\mathbf{x}}} \log(p_{\sigma_0}(\tilde{\mathbf{x}}))$. Specifically, the objective is 1 and we just restate it here:

$$L_{SM}(\theta) = \mathbb{E}_{p_{\sigma_0}(\tilde{\mathbf{x}})} \|\nabla_{\tilde{\mathbf{x}}} \log(p_{\sigma_0}(\tilde{\mathbf{x}})) + \nabla_{\tilde{\mathbf{x}}} E(\tilde{\mathbf{x}}; \theta)\|^2 \quad (10)$$

Our key observation is: in high-dimensional space, due to the concentration of measure, the expectation w.r.t. $p_{\sigma_0}(\tilde{\mathbf{x}})$ over weighs a thin shell at roughly distance $\sqrt{d}\sigma$ to the empirical distribution $p(\mathbf{x})$. Though in theory this is not a problem, in practice this leads to results that the score are only well matched on this shell. Based on this observation, we suggest to replace the expectation w.r.t. $p_{\sigma_0}(\tilde{\mathbf{x}})$ with a multi-scale distribution $p_{\sigma'}(\tilde{\mathbf{x}})$, specifically, we choose $q_{\sigma'}(\tilde{\mathbf{x}}|\mathbf{x})$ to be a Gaussian scale mixture (Wainwright and Simoncelli, 2000) and $p_{\sigma'}(\tilde{\mathbf{x}}) = \int q_{\sigma'}(\tilde{\mathbf{x}}|\mathbf{x})p(\mathbf{x})d\mathbf{x}$. We call this *annealed score matching* and the objective is the following:

$$L_{ASM}(\theta) = \mathbb{E}_{p_{\sigma'}(\tilde{\mathbf{x}})} \|\nabla_{\tilde{\mathbf{x}}} \log(p_{\sigma_0}(\tilde{\mathbf{x}})) + \nabla_{\tilde{\mathbf{x}}} E(\tilde{\mathbf{x}}; \theta)\|^2 \quad (11)$$

Proposition 1. $L_{ASM}(\theta) = 0 \iff L_{SM}(\theta) = 0 \iff \theta = \theta^*$.

Given that $p_{\sigma'}(\tilde{\mathbf{x}})$ and $p_{\sigma_0}(\tilde{\mathbf{x}})$ has the same support, it's clear that $L_{ASM} = 0$ would be equivalent to $L_{SM} = 0$. Due to the proof of the Theorem 2 in Hyvärinen (2005), we have $L_{SM}(\theta) \iff \theta = \theta^*$. Thus, $L_{ASM}(\theta) = 0 \iff \theta = \theta^*$.

□

Proposition 2. $L_{ASM}(\theta) \smile L_{ADSM^*} = \mathbb{E}_{p_{\sigma'}(\tilde{\mathbf{x}})q_{\sigma_0}(\mathbf{x}|\tilde{\mathbf{x}})} \|\nabla_{\tilde{\mathbf{x}}} \log(q_{\sigma_0}(\tilde{\mathbf{x}}|\mathbf{x})) + \nabla_{\tilde{\mathbf{x}}} E(\tilde{\mathbf{x}}; \theta)\|^2$.

We follow the same procedure as in Vincent (2011) to prove this result.

$$\begin{aligned}
 J_{ASM}(\theta) &= \mathbb{E}_{p_{\sigma'}(\tilde{\mathbf{x}})} \|\nabla_{\tilde{\mathbf{x}}} \log(p_{\sigma_0}(\tilde{\mathbf{x}})) + \nabla_{\tilde{\mathbf{x}}} E(\tilde{\mathbf{x}}; \theta)\|^2 \\
 &= \mathbb{E}_{p_{\sigma'}(\tilde{\mathbf{x}})} \|\nabla_{\tilde{\mathbf{x}}} E(\tilde{\mathbf{x}}; \theta)\|^2 + 2S(\theta) + C \\
 S(\theta) &= \mathbb{E}_{p_{\sigma'}(\tilde{\mathbf{x}})} \langle \nabla_{\tilde{\mathbf{x}}} \log(p_{\sigma_0}(\tilde{\mathbf{x}})), \nabla_{\tilde{\mathbf{x}}} E(\tilde{\mathbf{x}}; \theta) \rangle \\
 &= \int_{\tilde{\mathbf{x}}} p_{\sigma'}(\tilde{\mathbf{x}}) \langle \nabla_{\tilde{\mathbf{x}}} \log(p_{\sigma_0}(\tilde{\mathbf{x}})), \nabla_{\tilde{\mathbf{x}}} E(\tilde{\mathbf{x}}; \theta) \rangle d\tilde{\mathbf{x}} \\
 &= \int_{\tilde{\mathbf{x}}} p_{\sigma'}(\tilde{\mathbf{x}}) \langle \frac{\nabla_{\tilde{\mathbf{x}}} p_{\sigma_0}(\tilde{\mathbf{x}})}{p_{\sigma_0}(\tilde{\mathbf{x}})}, \nabla_{\tilde{\mathbf{x}}} E(\tilde{\mathbf{x}}; \theta) \rangle d\tilde{\mathbf{x}} \\
 &= \int_{\tilde{\mathbf{x}}} \frac{p_{\sigma'}(\tilde{\mathbf{x}})}{p_{\sigma_0}(\tilde{\mathbf{x}})} \langle \nabla_{\tilde{\mathbf{x}}} p_{\sigma_0}(\tilde{\mathbf{x}}), \nabla_{\tilde{\mathbf{x}}} E(\tilde{\mathbf{x}}; \theta) \rangle d\tilde{\mathbf{x}} \\
 &= \int_{\tilde{\mathbf{x}}} \frac{p_{\sigma'}(\tilde{\mathbf{x}})}{p_{\sigma_0}(\tilde{\mathbf{x}})} \langle \nabla_{\tilde{\mathbf{x}}} \int_{\mathbf{x}} p(\mathbf{x}) q_{\sigma_0}(\tilde{\mathbf{x}}|\mathbf{x}) d\mathbf{x}, \nabla_{\tilde{\mathbf{x}}} E(\tilde{\mathbf{x}}; \theta) \rangle d\tilde{\mathbf{x}} \\
 &= \int_{\tilde{\mathbf{x}}} \frac{p_{\sigma'}(\tilde{\mathbf{x}})}{p_{\sigma_0}(\tilde{\mathbf{x}})} \langle \int_{\mathbf{x}} p(\mathbf{x}) \nabla_{\tilde{\mathbf{x}}} q_{\sigma_0}(\tilde{\mathbf{x}}|\mathbf{x}) d\mathbf{x}, \nabla_{\tilde{\mathbf{x}}} E(\tilde{\mathbf{x}}; \theta) \rangle d\tilde{\mathbf{x}} \\
 &= \int_{\tilde{\mathbf{x}}} \frac{p_{\sigma'}(\tilde{\mathbf{x}})}{p_{\sigma_0}(\tilde{\mathbf{x}})} \langle \int_{\mathbf{x}} p(\mathbf{x}) q_{\sigma_0}(\tilde{\mathbf{x}}|\mathbf{x}) \nabla_{\tilde{\mathbf{x}}} \log q_{\sigma_0}(\tilde{\mathbf{x}}|\mathbf{x}) d\mathbf{x}, \nabla_{\tilde{\mathbf{x}}} E(\tilde{\mathbf{x}}; \theta) \rangle d\tilde{\mathbf{x}} \\
 &= \int_{\tilde{\mathbf{x}}} \int_{\mathbf{x}} \frac{p_{\sigma'}(\tilde{\mathbf{x}})}{p_{\sigma_0}(\tilde{\mathbf{x}})} p(\mathbf{x}) q_{\sigma_0}(\tilde{\mathbf{x}}|\mathbf{x}) \langle \nabla_{\tilde{\mathbf{x}}} \log q_{\sigma_0}(\tilde{\mathbf{x}}|\mathbf{x}), \nabla_{\tilde{\mathbf{x}}} E(\tilde{\mathbf{x}}; \theta) \rangle d\tilde{\mathbf{x}} d\mathbf{x} \\
 &= \int_{\tilde{\mathbf{x}}} \int_{\mathbf{x}} \frac{p_{\sigma'}(\tilde{\mathbf{x}})}{p_{\sigma_0}(\tilde{\mathbf{x}})} p_{\sigma_0}(\tilde{\mathbf{x}}, \mathbf{x}) \langle \nabla_{\tilde{\mathbf{x}}} \log q_{\sigma_0}(\tilde{\mathbf{x}}|\mathbf{x}), \nabla_{\tilde{\mathbf{x}}} E(\tilde{\mathbf{x}}; \theta) \rangle d\tilde{\mathbf{x}} d\mathbf{x} \\
 &= \int_{\tilde{\mathbf{x}}} \int_{\mathbf{x}} p_{\sigma'}(\tilde{\mathbf{x}}) q_{\sigma_0}(\mathbf{x}|\tilde{\mathbf{x}}) \langle \nabla_{\tilde{\mathbf{x}}} \log q_{\sigma_0}(\tilde{\mathbf{x}}|\mathbf{x}), \nabla_{\tilde{\mathbf{x}}} E(\tilde{\mathbf{x}}; \theta) \rangle d\tilde{\mathbf{x}} d\mathbf{x}
 \end{aligned}$$

Thus we have:

$$\begin{aligned}
 L_{ASM}(\theta) &= \mathbb{E}_{p_{\sigma'}(\tilde{\mathbf{x}})} \|\nabla_{\tilde{\mathbf{x}}} E(\tilde{\mathbf{x}}; \theta)\|^2 + 2S(\theta) + C \\
 &= \mathbb{E}_{p_{\sigma'}(\tilde{\mathbf{x}})q_{\sigma_0}(\mathbf{x}|\tilde{\mathbf{x}})} \|\nabla_{\tilde{\mathbf{x}}} E(\tilde{\mathbf{x}}; \theta)\|^2 + 2\mathbb{E}_{p_{\sigma'}(\tilde{\mathbf{x}})q_{\sigma_0}(\mathbf{x}|\tilde{\mathbf{x}})} \langle \nabla_{\tilde{\mathbf{x}}} \log q_{\sigma_0}(\tilde{\mathbf{x}}|\mathbf{x}), \nabla_{\tilde{\mathbf{x}}} E(\tilde{\mathbf{x}}; \theta) \rangle + C \\
 &= \mathbb{E}_{p_{\sigma'}(\tilde{\mathbf{x}})q_{\sigma_0}(\mathbf{x}|\tilde{\mathbf{x}})} \|\nabla_{\tilde{\mathbf{x}}} \log(q_{\sigma_0}(\tilde{\mathbf{x}}|\mathbf{x})) + \nabla_{\tilde{\mathbf{x}}} E(\tilde{\mathbf{x}}; \theta)\|^2 + C'
 \end{aligned}$$

So $L_{ASM}(\theta) \smile L_{ADSM^*}$.

□

By Proposition 1 and Proposition 2, we have the following form to optimize:

$$\begin{aligned}
 L_{ADSM^*}(\theta) &= \int_{\tilde{\mathbf{x}}} \int_{\mathbf{x}} p_{\sigma'}(\tilde{\mathbf{x}}) q_{\sigma_0}(\mathbf{x}|\tilde{\mathbf{x}}) \|\nabla_{\tilde{\mathbf{x}}} \log(q_{\sigma_0}(\tilde{\mathbf{x}}|\mathbf{x})) + \nabla_{\tilde{\mathbf{x}}} E(\tilde{\mathbf{x}}; \theta)\|^2 d\tilde{\mathbf{x}} d\mathbf{x} \\
 &= \int_{\tilde{\mathbf{x}}} \int_{\mathbf{x}} \frac{q_{\sigma_0}(\mathbf{x}|\tilde{\mathbf{x}})}{q_{\sigma'}(\mathbf{x}|\tilde{\mathbf{x}})} p_{\sigma'}(\tilde{\mathbf{x}}) q_{\sigma'}(\mathbf{x}|\tilde{\mathbf{x}}) \|\nabla_{\tilde{\mathbf{x}}} \log(q_{\sigma_0}(\tilde{\mathbf{x}}|\mathbf{x})) + \nabla_{\tilde{\mathbf{x}}} E(\tilde{\mathbf{x}}; \theta)\|^2 d\tilde{\mathbf{x}} d\mathbf{x} \\
 &= \int_{\tilde{\mathbf{x}}} \int_{\mathbf{x}} \frac{q_{\sigma_0}(\mathbf{x}|\tilde{\mathbf{x}})}{q_{\sigma'}(\mathbf{x}|\tilde{\mathbf{x}})} p_{\sigma'}(\mathbf{x}, \tilde{\mathbf{x}}) \|\nabla_{\tilde{\mathbf{x}}} \log(q_{\sigma_0}(\tilde{\mathbf{x}}|\mathbf{x})) + \nabla_{\tilde{\mathbf{x}}} E(\tilde{\mathbf{x}}; \theta)\|^2 d\tilde{\mathbf{x}} d\mathbf{x} \\
 &= \int_{\tilde{\mathbf{x}}} \int_{\mathbf{x}} \frac{q_{\sigma_0}(\mathbf{x}|\tilde{\mathbf{x}})}{q_{\sigma'}(\mathbf{x}|\tilde{\mathbf{x}})} q_{\sigma'}(\tilde{\mathbf{x}}|\mathbf{x}) p(\mathbf{x}) \|\nabla_{\tilde{\mathbf{x}}} \log(q_{\sigma_0}(\tilde{\mathbf{x}}|\mathbf{x})) + \nabla_{\tilde{\mathbf{x}}} E(\tilde{\mathbf{x}}; \theta)\|^2 d\tilde{\mathbf{x}} d\mathbf{x} \quad (*) \\
 &= L_{ADM}(\theta)
 \end{aligned}$$

To minimize Equation (*), we can use the following importance sampling procedure (Russell and Norvig, 2016): we can sample from the empirical distribution $p(\mathbf{x})$, then sample the Gaussian scale mixture $q_{\sigma'}(\tilde{\mathbf{x}}|\mathbf{x})$ and finally weight the sample by $\frac{q_{\sigma_0}(\mathbf{x}|\tilde{\mathbf{x}})}{q_{\sigma'}(\mathbf{x}|\tilde{\mathbf{x}})}$. We expect the ratio to be close to 1 because in $\tilde{\mathbf{x}}$ is generated by adding Gaussian noise to real data sample, and the estimator $q_{\sigma_0}(\mathbf{x}|\tilde{\mathbf{x}})$ and $q_{\sigma'}(\mathbf{x}|\tilde{\mathbf{x}})$ should give very similar distribution over \mathbf{x} . Therefore, in practice, we ignore the weighting factor and use Equation 5.

C PROBLEM WITH SINGLE NOISE DENOISING SCORE MATCHING

To compare with previous method, we trained energy-based model with denoising score matching using one noise level on MNIST, initialized the sampling with Gaussian noise of the same level, and sampled with Langevin dynamics at $T = 1$ for 1000 steps and perform one denoise jump to recover the model’s best estimate of the clean sample, see Figure C.1. We used the same 12-layer ResNet as other MNIST experiments. Models were trained for 100000 steps before sampling.



Figure C.1: Denoised samples from energy-based model trained with denoising score matching with single magnitude Gaussian noise on MNIST. Noise magnitude used in training is shown above samples.

D OVERFITTING TEST

We demonstrate that the model does not simply memorize training examples by comparing model samples with their nearest neighbors in the training set. We use Fashion MNIST for this demonstration because overfitting can occur there easier than on more complicated datasets, see Figure D.1.

E DETAILS ON TRAINING AND SAMPLING

We used a custom designed ResNet architecture for all experiments. For MNIST and Fashion-MNIST we used a 12-layer ResNet with 64 filters on first layer, while for CelebA and CIFAR dataset we used a 18-layer ResNet with 128 filters on the first layer. All network used the ELU activation function. We did not use any normalization in the ResBlocks and the filter number is doubled at each downsampling block. Details about the structure of our networks used can be found in our code release [Here](#). All mentioned models can be trained on 2 GPUs within 2 days.

Since the gradient of our energy model scales linearly with the noise, we expected our energy function to scale quadratically with noise magnitude. Therefore, we modified the standard energy-based network output layer to take a flexible quadratic form (Fan et al., 2018):

$$E_{out} = \left(\sum_i a_i h_i + b_1 \right) \left(\sum_i c_i h_i + b_2 \right) + \sum_i d_i h_i^2 + b_3 \quad (12)$$

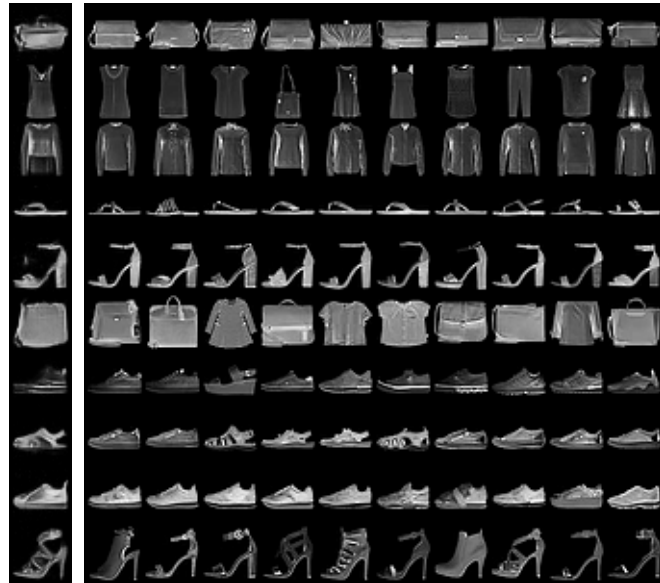


Figure D.1: Samples from energy-based model trained on Fashion MNIST (Left column) next to 10 (L2) nearest neighbors in the training set.

where a_i, c_i, d_i and b_1, b_2, b_3 are learnable parameters, and h_i is the (flattened) output of last residual block. We found this modification to significantly improve performance compared to using a simple linear last layer.

For CIFAR and CelebA results we trained for 300k weight updates, saving a checkpoint every 5000 updates. We then took 1000 samples from each saved networks and used the network with the lowest FID score. For MNIST and fashion MNIST we simply trained for 100k updates and used the last checkpoint. During training we pad MNIST and Fashion MNIST to 32*32 for convenience and randomly flipped CelebA images. No other modification was performed. We only constrained the gradient of the energy function, the energy value itself could in principle be unbounded. However, we observed that they naturally stabilize so we did not explicitly regularize them. The annealing sampling schedule is optimized to improve sample quality for CIFAR-10 dataset, and consist of a total of 2700 steps. For other datasets the shape has less effect on sample quality, see Figure G.1 B for the shape of annealing schedule used.

For the Log likelihood estimation we initialized reverse chain on test images, then sample 10000 intermediate distribution using 10 steps HMC updates each. Temperature schedule is roughly exponential shaped and the reference distribution is an isotropic Gaussian. The variance of estimation was generally less than 10% on the log scale. Due to the high variance of results, and to avoid getting dominated by a single outlier, we report average of the log density instead of log of average density.

F EXTENDED SAMPLES AND INPAINTING RESULTS

We provide more inpainting examples and further demonstrate the mixing during sampling process in Figure F.1. We also provide more samples for readers to visually judge the quality of our sample generation in Figure F.2, F.3 and F.4. All samples are randomly selected.

G SAMPLING PROCESS AND ENERGY VALUE COMPARISONS

Here we show how the average energy of samples behaves vs the sampling temperature. We also show an example of our model making out of distribution error that is common in most other likelihood based models (Nalisnick et al., 2019) Figure G.1.

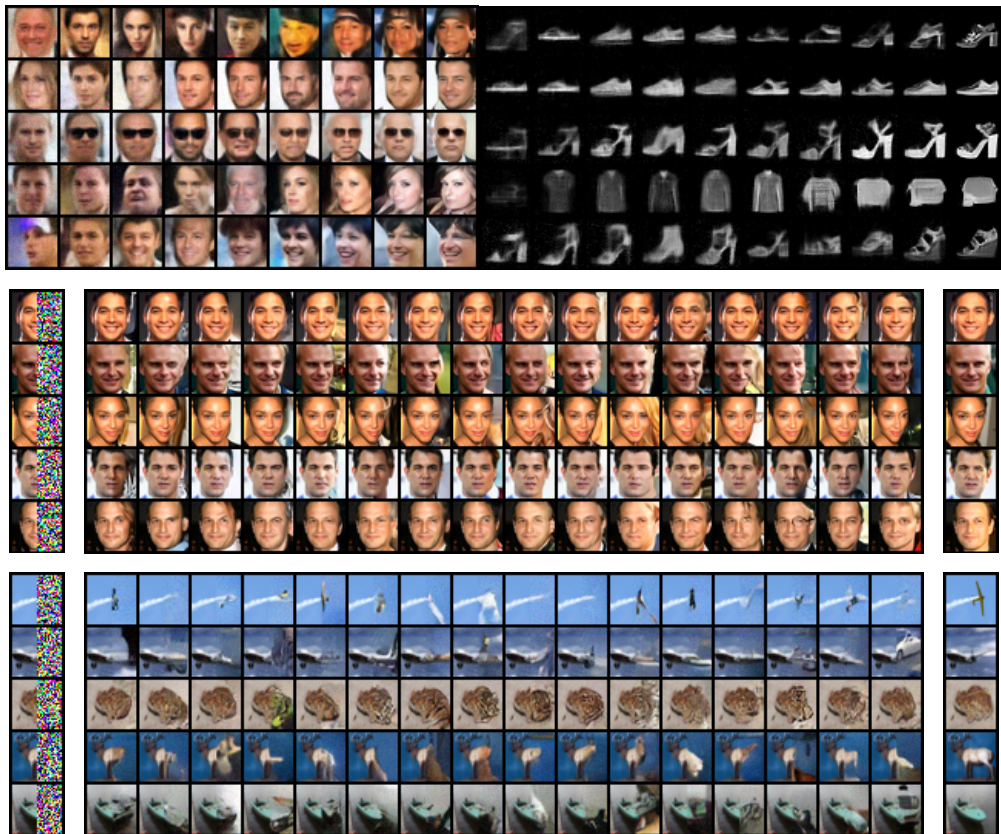


Figure F.1: Denoised Sampling process and inpainting results. Sampling process is from left to right.

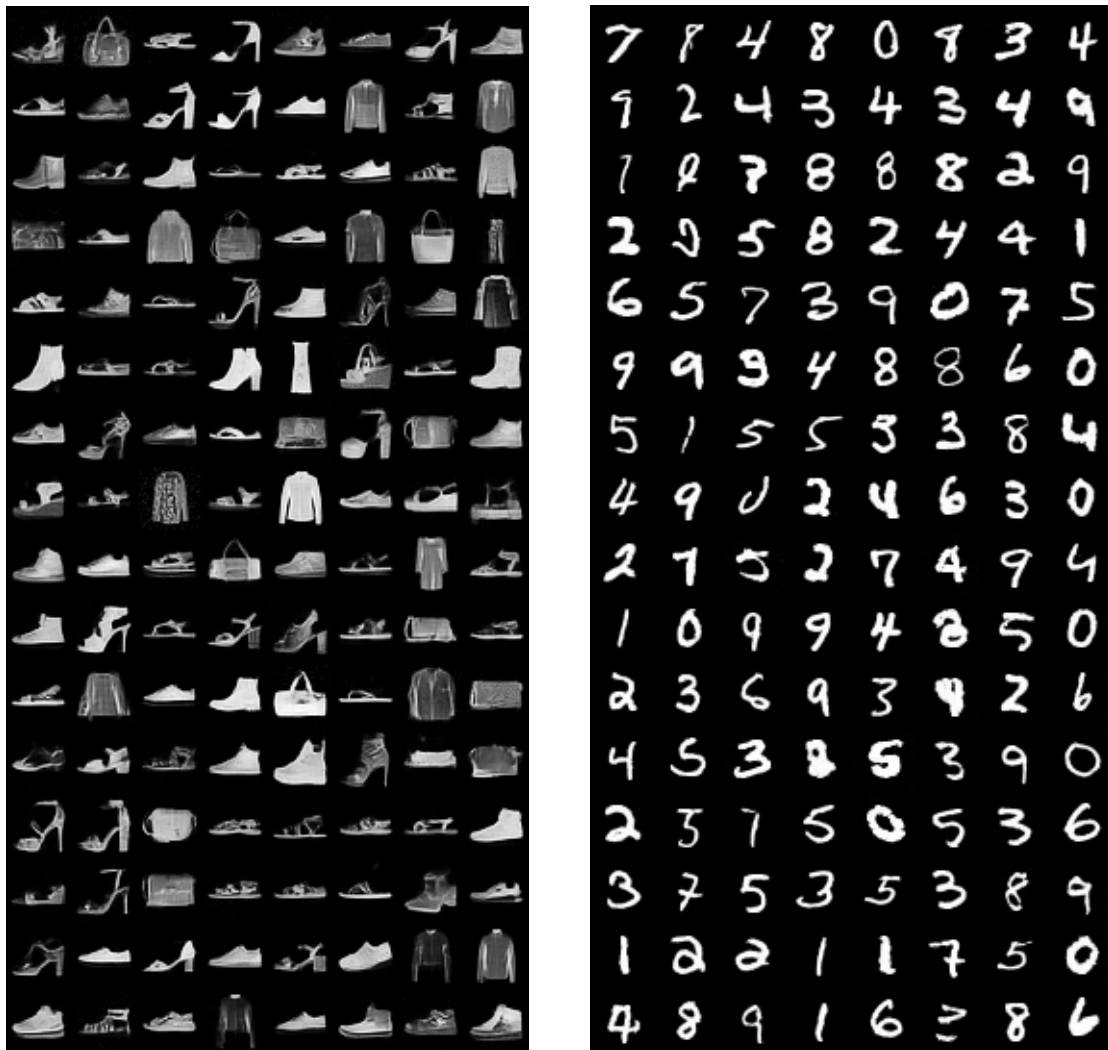


Figure F.2: Extended Fashion MNIST and MNIST samples



Figure F.3: Samples (left panel) from network trained on CelebA, and training examples from the dataset (right panel).

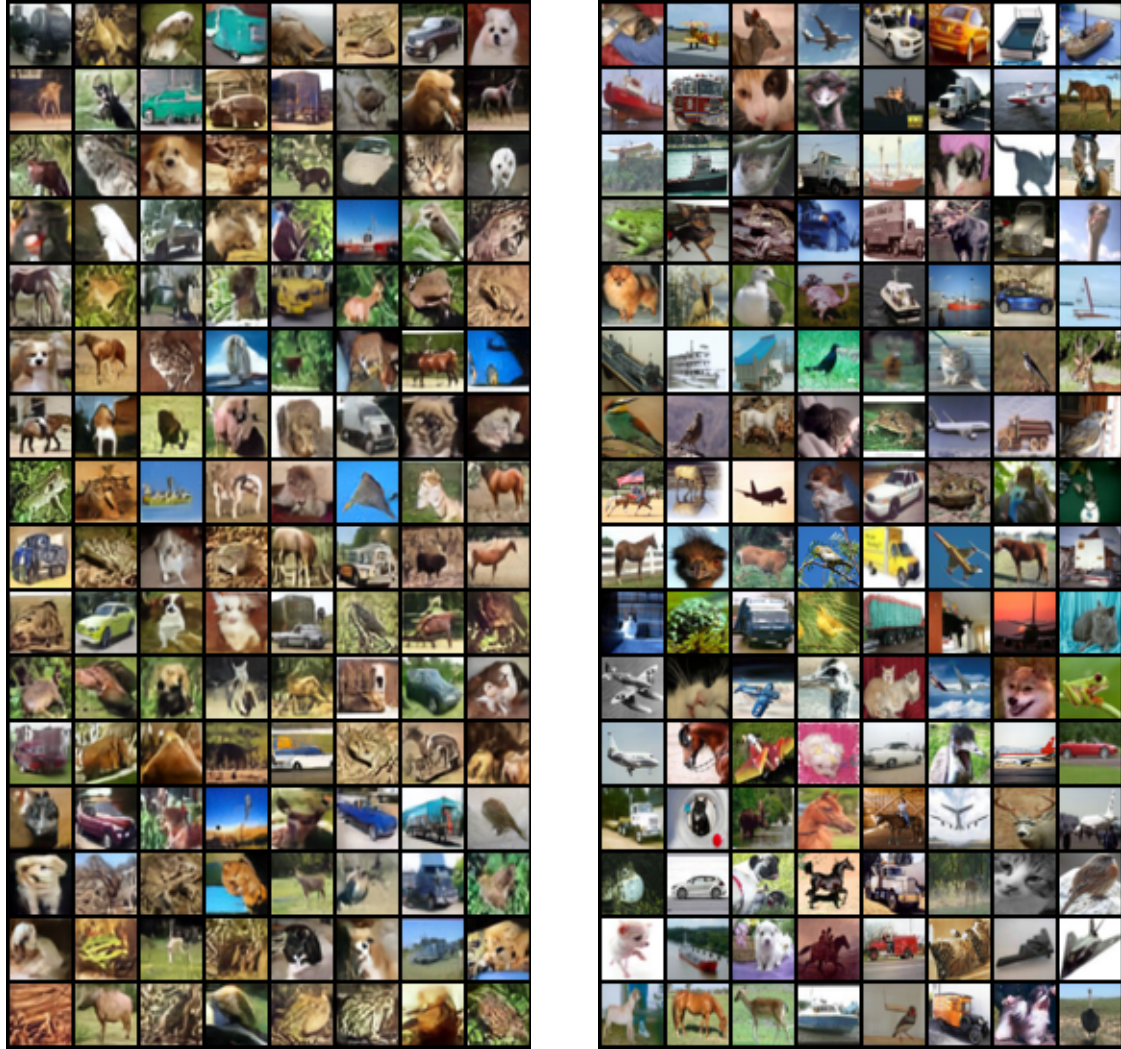


Figure F.4: Samples (left panel) from energy-based model trained on CIFAR-10 next to training examples (right panel).

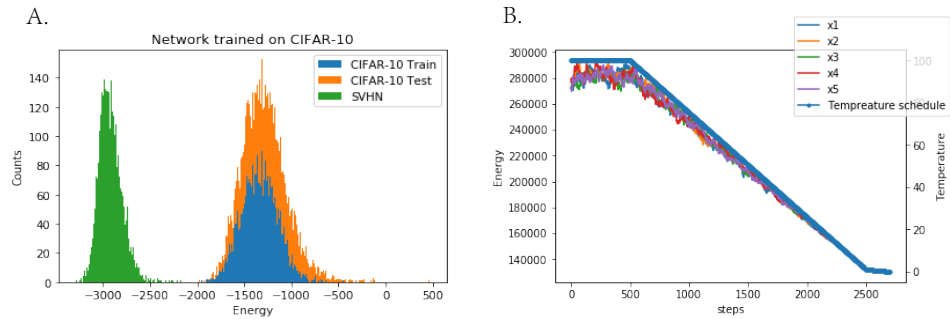


Figure G.1: A. Energy values for CIFAR-10 train, CIFAR-10 test and SVHN datasets for a network trained on CIFAR-10 images. Note that the network does not over fit to the training set, but just like most deep likelihood model, it assigns lower energy to SVHN images than its own training data. B. Annealing schedule and a typical energy trace for a sample during Annealed Langevin Sampling. The energy of the sample is proportional to the temperature, indicating sampling is close to a quasi-static process.